Composites

Effects of glycine on mechanical properties and microstructure of diamond-reinforced Ni nanocomposite coatings

Yanheng Zhang[1] , Lu Feng[1,2,*] , and Wei Qiu[1,2,*]

[1] *Department of Mechanics, Tianjin University, Tianjin 300354, China*
[2] *Tianjin Key Laboratory of Modern Engineering Mechanics, Tianjin 300354, China*

ABSTRACT

The diamond-reinforced Ni nanocomposite coatings were fabricated by a co-electrodeposition technique from a modified Watts-type bath in the presence of the organic additive glycine. Then, the effects of glycine on the morphology, microstructure, and mechanical properties of composite coatings were investigated based on scanning electron microscopy, energy-dispersive X-ray spectroscopy, X-ray diffraction analysis, hardness testing, and wear testing. By optimizing the glycine concentration, the incorporation of diamond particles was increased from 8.07 to 15.53% at%, while the size of nickel crystallites decreased with increasing glycine content to a smallest size of 15 nm. The relationship between the glycine concentration, microstructure, and mechanical properties including microhardness and wear resistance of the composite coatings was examined. The coatings hardness increased from 280 to 580 HV as the glycine concentration increased from 0 to 10 g L^{-1}. These increases in hardness were attributed to an increase in the content of embedded diamond particles in the coatings and the decrease in the nickel grain size. The friction and wear properties were evaluated as the concentration of glycine was optimized, showing a decrease in the wear volume from 37.8×10^{-3} to 17.9×10^{-3} mm^3. The wear resistance of the composite coatings increased as the glycine content was increased to an optimum value of 10 g L^{-1}, beyond which wear resistance decreased. Finally, a potential mechanism was proposed for explaining the effects of glycine on the microstructure and mechanical properties of the Ni–diamond nanocomposite coatings.

Address correspondence to E-mail: lufeng@tju.edu.cn; qiuwei@tju.edu.cn

 Springer

Introduction

Particle-reinforced metal matrix composites have a wide range of engineering applications owing to their high hardness, good wear resistance, and corrosion resistance compared with those features of pure metals or alloys [1, 2]. Rapid developments in composite materials have seen many reports published related to the preparation and performance of composite coatings [3–5]. The composite particle type, size, content, and interface of the composite coatings markedly affect the properties and applications of composite coatings [6, 7]. Several metals, including nickel, chromium, zinc, cobalt, and their alloys (e.g., Ni–W, Ni–Co, Ni–Fe), have been used as metallic matrices [8–10]. Notably, nickel has been recently developed and widely used in engineering parts as a protective coating with high tensile strength, good toughness, and wear resistance. Hence, nickel is a candidate for replacing environmentally hazardous hexavalent chromium hard coatings [5, 11]. A nickel matrix can be further modified by a second reinforcing phase, which is made up of fine hard particles composed of metallic or nonmetallic compounds. Typical particles include alumina [8, 12–14], SiC [7, 15, 16], diamond [6, 17, 18], and ceria [19–21]. Among them, diamond has the highest hardness [22, 23], such that micro/nano-sized diamond particles are ideal reinforcing phases for enhancing coating hardness and wear resistance [18].

A nickel-based diamond composite coating with diamond as the dispersed phase and nickel as the matrix phase can be used as a wear-resistant coating in the aerospace industry, and in tools for grinding or cutting hard materials [17, 24]. Ni–diamond composite coatings maintain a sharp working surface, which has seen doping of diamond particles into diamond wire saws, grinding tools, drills, and other grinding or cutting tools for working hard materials, such as gemstones, jade articles, and ceramics [1]. In recent years, as technology for creating synthetic diamond has matured, the production costs of diamond particles have decreased considerably. These developments are particularly meaningful for research on preparation and performance of nickel-based diamond composite coatings [25].

Composite electrodeposition is a method of co-depositing a second phase of fine particles within a growing metal or alloy matrix during an electroplating process [5]. The co-electrodeposition technique has been extensively developed, owing to its relatively low operation costs and low processing temperatures [24, 26]. In this process, particles are suspended in a conventional plating electrolyte and captured into the growing metal coatings by mechanical stirring and electric field. The properties of composite coatings strongly depend on the content of particles incorporated during the deposition [1, 27]. Incorporation of more inert particles and more uniform distribution of the particles in a nickel matrix can improve the mechanical, tribological, anti-corrosion, and anti-oxidation properties of the composite coatings [11, 28]. However, the incorporation and distribution of co-deposited particles are affected by processing parameters, such as particle characteristics (particle shape, size, concentration, and surface charge), bath composition (concentration, additives, and type and concentration of the active agent), current (current type and current density), bath temperature, and pH [25–27]. Among various influencing factors, the type and content of additives have a distinct influence on the electrodeposition process and coating performance [13, 17, 29]. There exist quite a few works applying new additives to Ni–diamond co-electroplating baths [17, 30]. For instance, Chuang et al. [17] studied the effects of propargyl alcohol and found that the dispersion of diamond particles and adhesion between the particles and substrate were improved by the addition of propargyl alcohol to the Ni–diamond composite electroplating bath. The corresponding coatings presented good leveling properties and reliable cutting performance. Choi et al. [30] demonstrated that the addition of S-based additives favored the dispersion of the diamond particles and improved the particles adhesion properties, which in turn increased the surface resistance.

As an organic additive, glycine has been applied to prepare pure nickel coatings since the last century [30, 31]. The ionized components of glycine in the plating solution can form complexes with the nickel ions, affecting the electrochemical process of nickel deposition [32]. A high glycine concentration might increase the cathode polarization of nickel electrodeposition [33], thereby improving the surface topography and hardness of the coating [34]. Accordingly, the effects of glycine on the performance of Ni–diamond composite coatings should also be important [17]. Nevertheless, there have been no reports on the application of glycine to plating

solution for Ni–diamond electrodeposition to date, let alone characterize the mechanical behaviors of the corresponding composite coatings. The mechanism by which glycine alters the performance of nickel-based diamond composite coating is also unknown. Therefore, the aim of this paper is to investigate and examine the effects of glycine on the microstructure and mechanical properties of Ni–diamond composite coatings.

In the present research, glycine was introduced into a widely used Watts-type bath as a novel organic additive, and the co-electrodeposition of the Ni–diamond composite coating was achieved from the nickel plating bath containing diamond particles in suspension. The effects of glycine on the microstructure and mechanical properties of the composite coatings were obtained by various surface analysis techniques. Furthermore, combined with the effect of glycine on the composition of plating solution, the function of glycine during the preparation of nickel-based diamond composite coatings and the effect mechanism of glycine on the mechanical properties of the composite coatings were both revealed.

Experimental

Electrodeposition procedure

The bath composition and deposition parameters are outlined in Table 1. A basic Watts-type nickel plating solution ($NiSO_4 \cdot 6H_2O$ 240 g L^{-1}, $NiCl_2 \cdot 6H_2O$

Table 1 Chemical composition of the electrodeposition bath and the operating conditions

Components/parameters	
$NiSO_4 \cdot 6H_2O$	240 g L^{-1}
$NiCl_2 \cdot 6H_2O$	40 g L^{-1}
H_3BO_3	30 g L^{-1}
Saccharin	1 g L^{-1}
Sodium dodecyl sulfate	0.1 g L^{-1}
Diamond particles	15 g L^{-1}
Particle size of diamonds	1 μm
Glycine	0, 2, 5, 10, 15 g L^{-1}
pH	4.0
Temperature	50 °C
Current density	4 A dm^{-2}
Stirring rate	500 rpm
Deposition time	30 min

40 g L^{-1}, H_3BO_3 30 g L^{-1}) containing a few additives (saccharin, sodium lauryl sulfate) was used, and the additive glycine was added at 0, 2, 5, 10, and 15 g L^{-1}, respectively. All solutions were prepared with analytic grade reagents and deionized water. The bath pH was adjusted to 4 by dripping the dilute sulfuric acid with 10% mass fraction and the NaOH solution with 10% mass fraction into the bath in proper order, and its temperature was maintained at 50 °C. A 304 stainless steel plate was used as substrate with an exposed surface of 20 mm × 15 mm defined by masking with insulation tape. The preparation process of composite coating is shown in Fig. 1. The steel plates were mechanically polished with #400, #800, #1200, and #2000 emery paper and then suspended for 5 min in a degreasing bath with Na_2CO_3 30 g L^{-1}, Na_3PO_4 30 g L^{-1}, NaOH 40 g L^{-1} at 70 °C. The plates were chemically etched in 10% H_2SO_4 at room temperature for 6 min to expose the contamination-free surface. After each of the pretreatment steps, the substrates were rinsed with deionized water and dried with an air flow.

The electroplating device and electrochemical process are shown in Fig. 2. A 250-mL beaker placed in a magnetic stirrer (LICHEN, DF-101S) at a stirring rate of 500 rpm was used as the plating bath, and the bath temperature was maintained at a constant. A nickel plate and steel were used as the anode and cathode, respectively, at a distance of 50 mm. The electrodeposition began after switching on the DC regulated power supply (LONGWEI, LW-3010KDS) accompanied by a current density of 4 A dm^{-2}. During the plating, the cations in the bath moved to the cathode surface under the electric field force and also partly adsorbed to diamond particles, such that the particles were also carried to the cathode surface and co-deposited. After 30 min, the co-deposition step was completed and the coated sample was ultrasonicated in deionized water for 5 min.
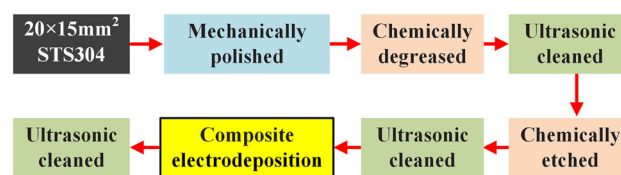

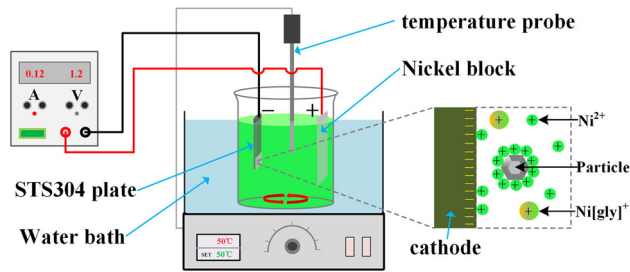**Figure 1** Process for preparing Ni–diamond composite coating.

Figure 2 Equipment and electrochemical process of Ni–diamond co-electrodeposition.

Instruments and methods

The macro-mechanical properties of Ni-based diamond composite coatings are strongly affected by their surface topography and structure, including the surface roughness, grain size, and the incorporation and distribution of diamond particles [1, 26, 28, 35]. The surface topography and chemical composition of the Ni–diamond films were studied with a scanning electron microscope (SEM, Phenom ProX, Dutch) combined with energy-dispersive X-ray spectroscopy (EDS). The distribution of diamond particles in the cross section of the multilayers was viewed with an optical microscope (OM, KH7700, Hirox, Japan). The three-dimensional surface topography and surface roughness of the composite coatings were measured with a three-dimensional profiler (ST400, NANO-VEA, USA). X-ray diffraction (XRD, D/MAX-2500, Rigaku, Japan) was performed at 40 kV, with Cu K_α radiation and a scan rate of 4°min^{-1} over the range between 0° and 90°. The preferred orientation and grain size of the matrix material were determined from the XRD patterns. Another X-ray diffraction analyzer (μ-X360s, Pulstec, Japan) which could collect 360° omnidirectional diffraction data to obtain a complete Debye ring from incident X-rays at a single angle with a self-equipped fully two-dimensional surface detector was used to fully analyze the preferred orientation and grain size of the nickel matrix. The instrument settings were 30 kV tube pressure, Cr K_β radiation, in the (311) diffraction direction, a test time of 120 s, and X-ray incidence angle of 35°. The thickness of the specimen before and after plating was measured with a digital micrometer (PD-151, Pro's Kit), and the difference was used to determine the coating thickness. The average value at five different randomly selected points was defined as the thickness of the composite coating.

The microhardness was analyzed using a microhardness tester (HXD-1000TMC/LCD, Shanghai Taiming Optical Instrument Co. Ltd., China) with a diamond pyramid indenter at a load of 200 g for 15 s, being widely used for nickel films [27, 36]. The average value of 10 different sampling points on the surface was defined as the microhardness of composite coating. The wear tests were performed by a reciprocating ball-on-disk tester (UMT-2, Bruker, Germany), connected to a computer monitoring the dynamic coefficient of friction (in both sliding directions), at room temperature and a relative humidity of 45–55% under dry sliding. An GCr15 stainless steel ball (diameter = 4 mm) was used as the counterpart, and the wear tests were performed for 30 min under a load of 3 N with a sliding speed of 0.020 m s^{-1}. Wear rates of all the coatings and counters were calculated on the basis of the volumetric loss, measured using a surface profilometer (Contour GT-K, Bruker, Germany). Wear rates of all the composite coatings were calculated using the equation $K = V (SF)^{-1}$, where V was the wear volume loss in mm^3, S, the total sliding distance in m, and F, the normal load in N.

Results

Surface morphology and composition of coatings

The effects of different glycine concentrations on the surface and cross-sectional morphology of the Ni–diamond composite coatings are shown in Fig. 3. The SEM images (Fig. 3a, b) indicate that the addition of glycine improves the coating surface flatness and the composite condition of diamond particles. The coated surface becomes smoother as the glycine content is increased, as shown in Fig. 3a–d. The coating with optimal surface morphology and most particle incorporation is achieved at a glycine concentration of 10 g L^{-1} (Fig. 3d). However, as shown in Fig. 3e, when the glycine additive concentration is increased to 15 g L^{-1}, bulges are formed by the accumulation of nickel grains and diamond particles, which result in a decrease in the coating flatness and surface quality. The cross-sectional OM images are shown in Fig. 3f–j. When there is no glycine, the amount of diamond particles is lower and the particle aggregations are obvious, indicating a weak particle strengthening
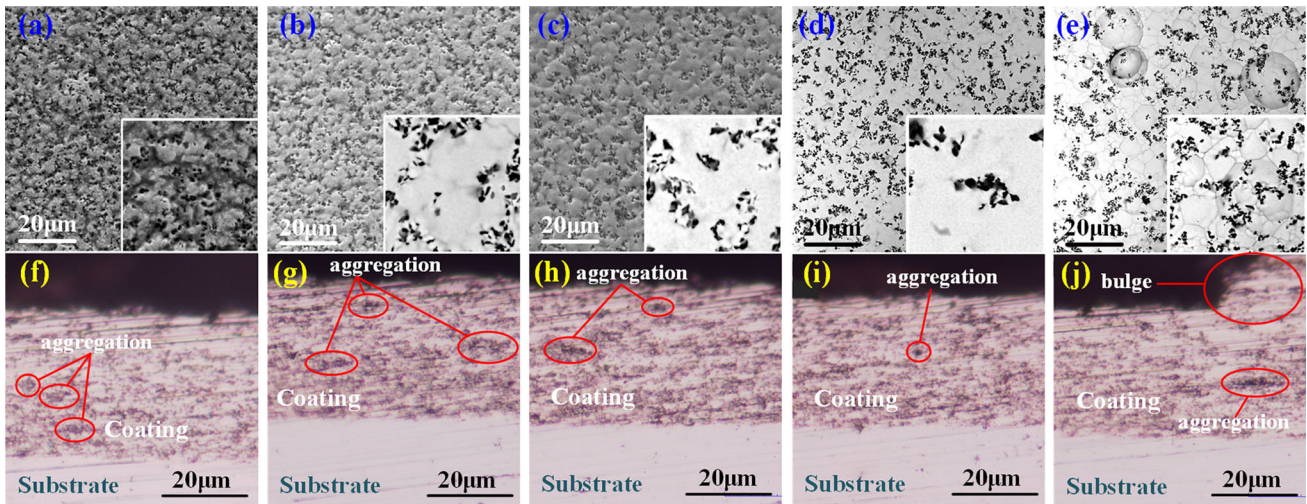
Figure 3 Surface SEM morphology of composite coatings prepared by different glycine contents: **a** 0 g L^{-1}, **b** 2 g L^{-1}, **c** 5 g L^{-1}, **d** 10 g L^{-1}, **e** 15 g L^{-1}; inset images show high-magnification SEM images of regions in **a**, **b**, **c**, **d**, and **e**, respectively; cross-sectional OM morphology of composite coatings prepared by different glycine contents: **f** 0 g L^{-1}, **g** 2 g L^{-1}, **h** 5 g L^{-1}, **i** 10 g L^{-1}, **j** 15 g L^{-1}.

effect, as shown in Fig. 3f. With the increase in glycine concentration, the composite amount of diamond particles increases obviously and the particle aggregations decrease, meaning an improved particle dispersion, as shown in Fig. 3g–i. The particle incorporation reaches optimal in the coating with glycine at 10 g L^{-1}, and the particle aggregations are least (Fig. 3i), indicating the best particle dispersion. However, as shown in Fig. 3j, excessive glycine leads to bigger particle aggregation in the coating and bulges on the corresponding coating surface, so the particle dispersion in the coating is the worst. The effect of glycine on the thickness of the composite coating is shown in Fig. 4. The coating thickness decreases as the glycine concentration is increased, which is consistent with the variation of coating thickness from the cross-sectional OM observation, as shown in Fig. 3f–j. This result further indicates that the change of glycine concentration affects the co-electrodeposition rate.

The EDS results of the coatings and the incorporation of diamond particles at different glycine concentrations are shown in Fig. 5. These results indicate that the coatings are composed of nickel and diamond, and the diamond content increases as the glycine concentration is increased. The highest diamond particle content is 15.53 at% at a glycine concentration of 10 g L^{-1}. However, when the concentration of glycine is increased further, diamond incorporation declines.
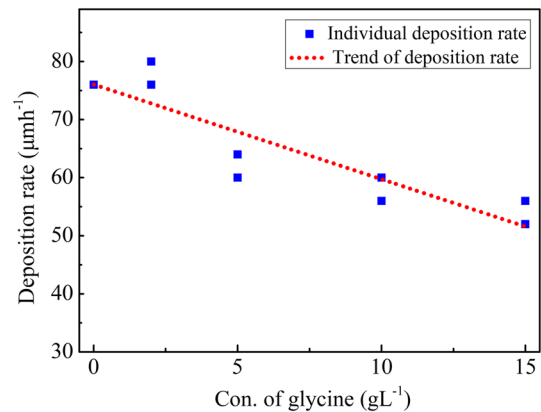

Figure 4 Effects of glycine on the deposition rate of composite coatings.

Surface roughness

The three-dimensional surface topography and roughness are evaluated as functions of the glycine concentration, as shown in Fig. 6 and Table 2, respectively.

These results show that increasing glycine concentration improves the coating flatness and reduces the surface roughness, as shown in Fig. 6a–d. However, excess glycine causes bump-like aggregations on the coating surface, which increase surface roughness, as shown in Fig. 6e. The composite coating has the lowest surface roughness when the glycine concentration is 10 g L^{-1}.

Figure 5 Diamond content in the Ni–diamond composite coatings measured by EDS fitted to a scanning electron microscope: **a** without glycine, **b** 5 g L^{-1} glycine, **c** 10 g L^{-1} glycine, **d** 15 g L^{-1} glycine.
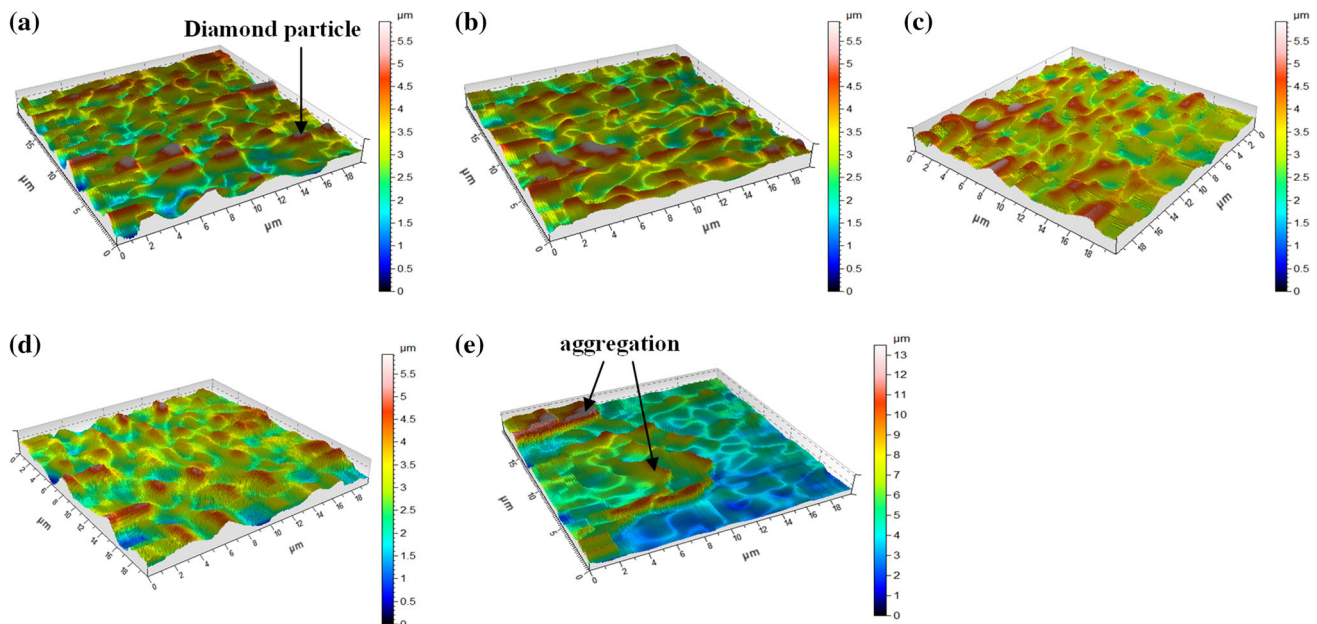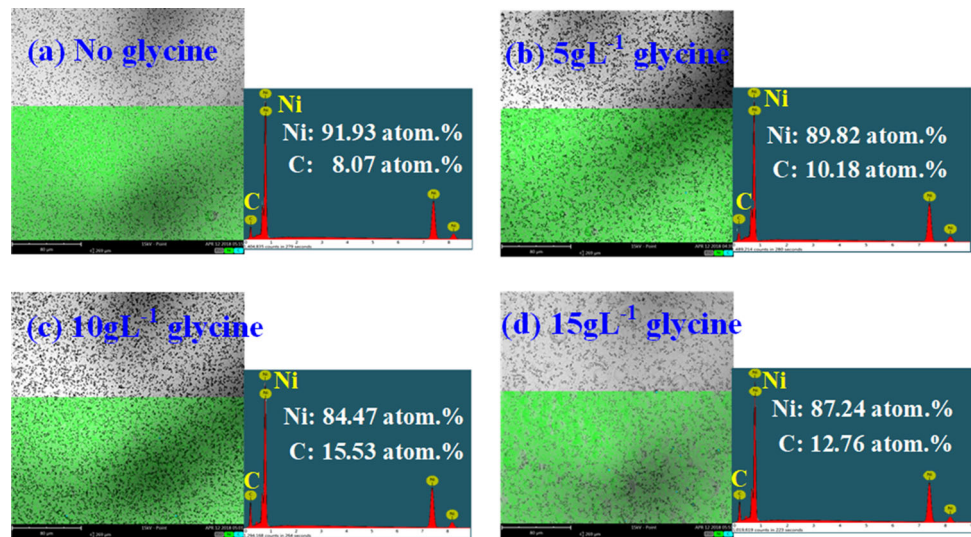

Figure 6 Surface roughness of Ni–diamond composite coating layer electrodeposited by addition of glycine: **a** 0 g L^{-1}, **b** 2 g L^{-1}, **c** 5 g L^{-1}, **d** 10 g L^{-1}, and **e** 15 g L^{-1}.

Table 2 Roughness average (R_a) of the surface of Ni–diamond composite coatings with added glycine

Concentration (g L^{-1})	0	2	5	10	15
R_a (μm)	0.7340	0.5898	0.5187	0.4765	1.5108
Std.dev. (μm)	0.0120	0.0305	0.0213	0.0037	0.3910

Microstructure

XRD patterns of the Ni–diamond composite coatings prepared with different glycine concentrations are illustrated in Fig. 7. The composite coatings exhibit typical face-centered cubic lattice of nickel with different orientations. The preferred crystal orientation of the grains in the polycrystalline nickel metal is the (111) and (200) crystal planes. The peak intensities of these two planes for the composite coating produced without glycine are stronger than those of the coatings prepared with glycine. However, the peak
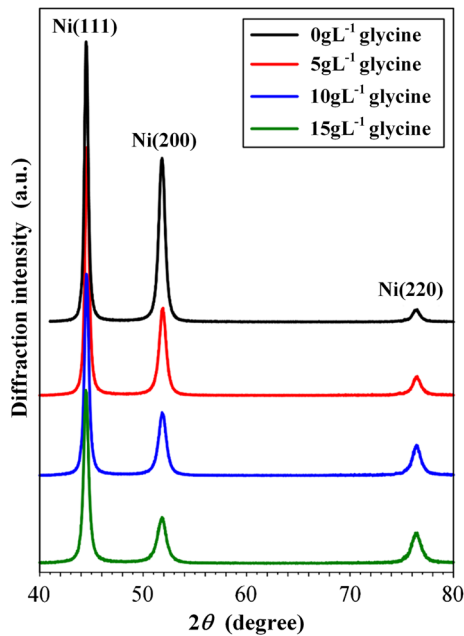
Figure 7 XRD patterns for composite coatings produced with different glycine concentrations in the plating bath.

Figure 8 Effects of glycine on the Ni grain size in Ni-diamond composite coatings.

intensities of the (111) and (200) planes decrease as the glycine concentration increases, whereas the peak intensity of the (220) plane increases slightly. Hence, the inner crystal orientations of the composite coatings become more random as the glycine concentration is increased.

Huis et al. [35] reported that the Scherrer XRD method and TEM observations are consistent in determining the mean cluster sizes. The Scherrer's equation [37], as Eq. 1 given, can be used to calculate the average grain sizes of the composite coatings prepared with various glycine contents.

$$D = \frac{0.9\lambda}{\beta \cos \theta} \tag{1}$$

where D is the main nickel grain size of the produced coating, λ is the wavelength radiation (0.154 nm), θ is the Bragg diffraction angle, and β is the full width at half maximum (FWHM).

By using Eq. 1, the nickel grain sizes of different composite coatings are achieved (shown in Fig. 8), which indicate that finer nano-sized matrix crystals are achieved by the addition of glycine and new crystallization sites form more rapidly when glycine is added to the plating bath. These results suggest that the additive glycine stimulates the nickel grain refinement.
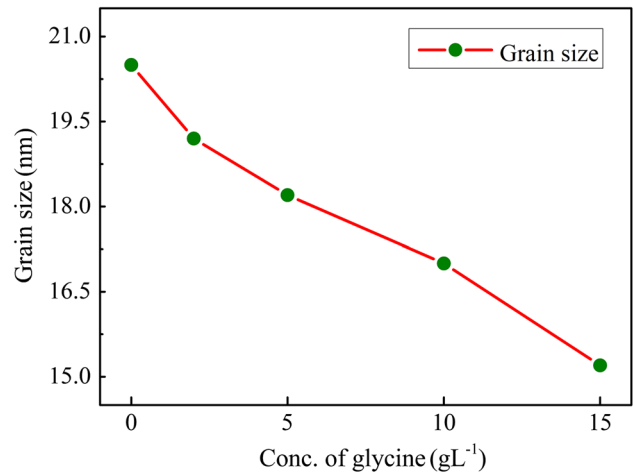
To further explore the influence of glycine on the microstructure of Ni–diamond composite coatings, the three-dimensional (3D) Debye–Scherrer rings are measured corresponding to the composite coatings prepared under different glycine concentrations (Fig. 9), where the color represents the diffraction intensity.

As shown in Fig. 9a, the Debye–Scherrer ring of the coating prepared without glycine is discontinuous, and the diffraction intensity is unevenly distributed along the circumference of the Debye–Scherrer ring, as shown in Fig. 10a. The distinct intensity of the Debye–Scherrer ring is clearly related to the texture of the specimen [38]. The uneven distribution of the diffraction peak FWHM indicates a large variation of the nickel grain size. Conversely, a smaller FWHM indicates a larger grain size. The XRD patterns shown in Fig. 7 show similar behavior.

As shown in Fig. 9b–e, the Debye–Scherrer rings with higher glycine concentration tend to be more continuous. Namely, the intensity of the Debye–Scherrer ring is evenly distributed along the circumference, shown in Fig. 10b, revealing a more randomly oriented polycrystalline material [38] (as for the results shown in Fig. 7). In this way, the lattice vacancy defects, which mainly concentrated on certain crystal planes, are reduced. Hence, the uniformity of the distribution of nickel atoms also
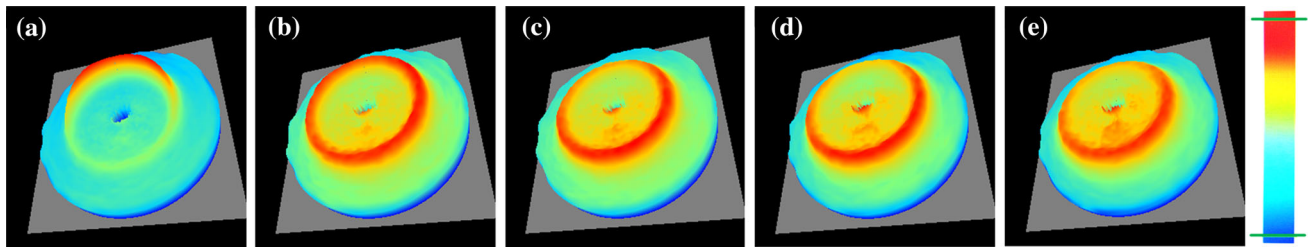
Figure 9 3D Debye–Scherrer rings of (311) diffraction plane from different specimens prepared by addition of glycine: **a** 0 g L^{-1}, **b** 2 g L^{-1}, **c** 5 g L^{-1}, **d** 10 g L^{-1}, and **e** 15 g L^{-1}.
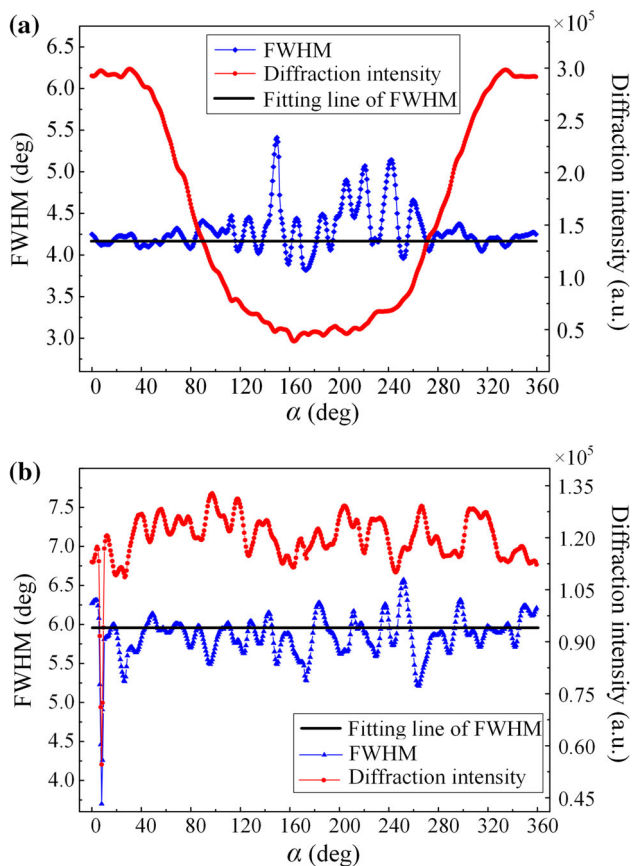

Figure 10 Distribution of diffraction peak intensity and FWHM of 3D Debye–Scherrer rings corresponding with coatings prepared by adding glycine: **a** 0 g L^{-1}, and **b** 10 g L^{-1}.

improved, which contributes to the enhanced micromechanical properties of the coatings [15]. Furthermore, the FWHM values of the diffraction peaks in Fig. 10b are more uniform and larger than those in Fig. 10a. Accordingly, the average nickel grain size is smaller, which is consistent with the varying trend of grain size shown in Fig. 8.

Microhardness

The effects of glycine on the microhardness of the pure Ni coatings and Ni–diamond composite coatings are shown in Fig. 11, showing that the addition of glycine increases the coatings microhardness. Furthermore, the microhardness gradually increases as the glycine concentration is increased. The highest microhardness of the composite coatings is 580 HV at a glycine concentration of 10 g L^{-1}. However, when the glycine concentration reaches 15 g L^{-1}, the microhardness decreases. Although the hardness of the pure nickel coating continues to increase, many bulges appear on the surface, and the hardness is much lower than that of the composite coating. Grain refinement based on the Hall–Patch effect can increase the coatings hardness [39], and it is likely one contribution of glycine to grain refinement (Fig. 9).
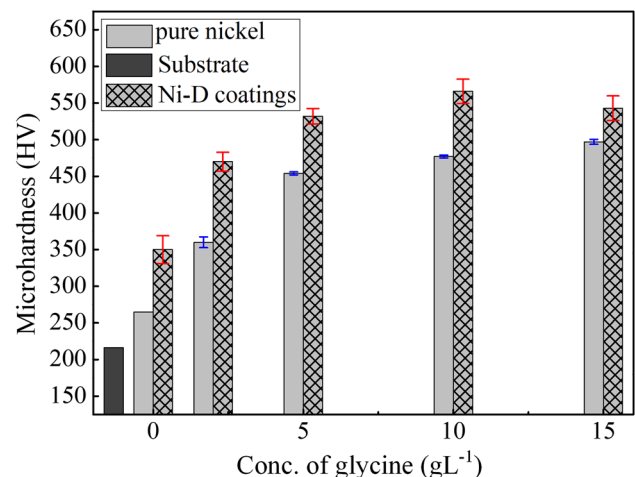

Figure 11 Effects of glycine on the microhardness of pure Ni coatings and Ni–diamond composite coatings.

Wear resistance

Friction curves of the composite coatings corresponding to different glycine concentrations under dry sliding conditions are shown in Fig. 12. The friction coefficient increases sharply during running in and then stabilizes to a steady state. The friction coefficient of the coating prepared without glycine is ~ 0.6. The addition of glycine decreases the friction coefficient to a minimum of ~ 0.4 at a glycine concentration of 10 g L^{-1}. The effects of glycine on the diamond content and wear rate of the composite coatings and bearing balls are shown in Fig. 13. The wear rates of the corresponding Ni–diamond composite coatings decrease as the glycine concentration in the plating bath is increased. The wear rate reaches the lowest when the glycine content is 10 g L^{-1}. The low wear rate of the composite coatings can be attributed to the dispersion-strengthening effect from the diamond particles incorporation (Fig. 13) [1, 40]. The material removal rate of the GCr15 steel ball bearing increases with increasing glycine content, and the removal rate of the ball on the composite coating prepared at 10 g L^{-1} of glycine is twice as high as that without glycine (Fig. 13), which indicates that the Ni–diamond composite coating, fabricated with added glycine, inhibits self-abrasion and increases cutting efficiency [1].

SEM has been used to study the wear surfaces of the co-deposited coatings prepared with different glycine concentrations as shown in Fig. 14. The wear
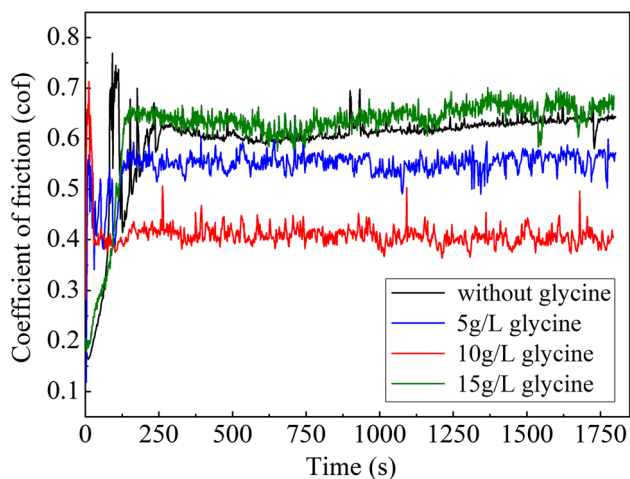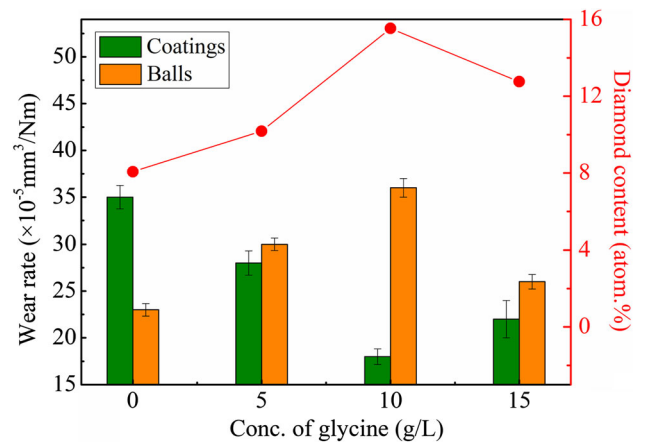

Figure 13 Effects of glycine on diamond content and wear rate of composite coatings and bearing balls.
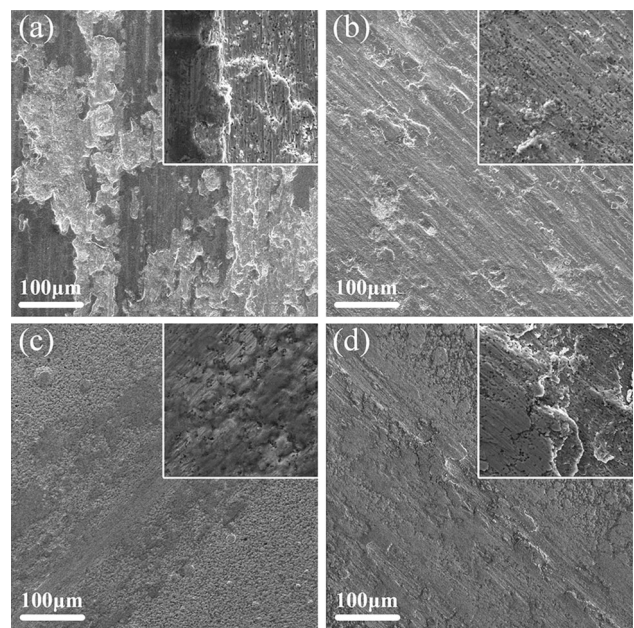

Figure 14 SEM images of the worn coating surfaces under dry sliding conditions corresponding to different glycine contents: **a** 0 g L^{-1}, **b** 5 g L^{-1}, **c** 10 g L^{-1}, and **d** 15 g L^{-1}. Inset images show **a**, **b**, **c**, and **d** at higher magnification.

Figure 12 Friction curves of the composite coatings prepared with different glycine concentrations under dry sliding condition.

tracks of the composite coatings show various scratches that contribute to wear loss [27]. Heavy peeling and delamination occur in the bulk during wear testing as shown by high-magnification SEM images of the wear surfaces of the composite coatings prepared without glycine (Fig. 14a), owing to the low adherence strength between the co-deposited layer and the substrate [6]. Nevertheless, the adhesion

wear and scuffing on the worn surfaces of the composite coatings decrease to some degree when glycine is added, particularly for the coating prepared with glycine at 10 g L^{-1}. Figure 14(c) shows narrower wear tracks and shallow discontinuous scratches, which are attributed to the dispersion strengthening by the higher content of diamond particles embedded in the composite coating (Fig. 12). Thus, the glycine increases the adhesion strength between the co-deposited layer and substrate. However, when the glycine concentration exceeds its optimum value, the brittleness of the metal matrix increases, and the deposited nickel is not able to bind all the particles tightly within the matrix. As a result, the counter body damages the coating surface and the anti-wear performance of the coatings decreases. The wear scar clearly demonstrates the wear resistance of the composite coatings [12], confirming that 10 g L^{-1} is the optimal glycine concentration for achieving the composite coating with the highest wear resistance. In comparing the effects of glycine on the hardness of the composite coatings (Fig. 11), the wear resistance follows the same varying trend, as described in the literature [2, 20].

Discussion

Effects of glycine on plating bath

Although glycine is usually presented as H$_2$N-CH$_2$-COOH, it is considered to be a dipolar ion (zwitterion) with a structure that protonates or deprotonates, depending on the solution pH [24]. In our research, the pH does not change during the plating process because the pH value of the bath was measured every 2 min by pH meter during the whole 0.5-h electrodeposition experiment, and the results showed that the pH value was kept at 4.0. When the pH of the plating solution is 4, the main structure of glycine ions under ionization equilibrium is H$_2$N-CH$_2$-COO$^-$, where lone pair electrons provided by the oxygen atom of the carboxyl group tend to occupy the empty orbit of Ni^{2+}, resulting in complexation between Ni^{2+} and Gly$^-$ [33]:

$$Ni^{2+} + Gly^- \rightarrow Ni[Gly]^+ \tag{2}$$

The main complex is highly dependent on the bath pH, and its structure changes little when pH is stable, regardless of the glycine concentration [41].

Visual MINTEQ, a software for the calculation of speciation, solubility, solid equilibrium, and minerals dissolved in aqueous solution under of chemical equilibrium [42], was applied to simulate the ion concentrations, pH, and temperature in the present work. The concentration of each component in the bath and the type and concentration of the complexes could be determined by setting the bath pH to 4, and the temperature to 50 °C, and then inputting the bath composition and its molar concentration. The calculation results illustrated that the main species of glycine was the complex [NiGly]$^+$, with negligible complexation between Ni^{2+} and saccharin, sodium dodecyl sulfate [43]. The effects of glycine on the molar ratio of Ni^{2+} and molar concentration of free glycine are shown in Fig. 15, which shows that the molar ratio of [NiGly]$^+$ and the concentration of glycine molecules increases almost linearly with the increase in glycine concentration, whereas the molar ratio of Ni^{2+} decreases. Furthermore, Ni^{2+} mainly exists as free cations rather than [NiGly]$^+$. Therefore, the main reduction reactions at the cathodes in the electrodeposition process are:

$$Ni^{2+} + 2e^- = Ni \tag{3}$$

$$Ni[Gly]^+ + 2e^- = Ni + H_2NCH_2COO^- \tag{4}$$

Effects of glycine on composite coating

Effects on deposition rate

The deposition efficiency of the composite coating is generally determined by the electrodeposition rate.
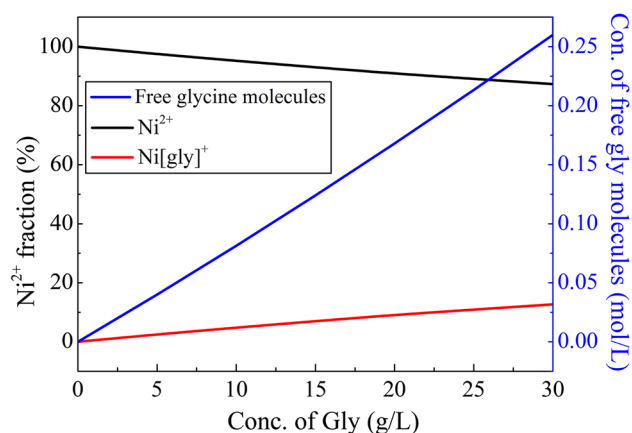

Figure 15 Effects of glycine on the molar ratio of Ni^{2+} and molar concentration of free glycine.

The effects of glycine on the electrodeposition rate are shown in Fig. 4. The deposition rate decreases as the glycine concentration is increased, whereas the electrodeposition rate of the plating layer depends on the ion concentration at the cathode surface [44].

Based on the experimental phenomena and results, a micromodel with electro-chemo-mechanical coupling is presented, shown in Fig. 16, to describe the electrochemical process on the cathode surface under different glycine concentrations. The trend described above (Fig. 4) might be attributed to the fact that, comparing with the case without glycine shown in Fig. 16a, complexation of Ni^{2+} with glycine reduced the nickel ion concentration at the cathode surface and suppressed the reduction reaction [11], which further decreased the electrodeposition rate, shown in Fig. 16b. In addition, a few free glycine molecules were adsorbed onto the cathode surface during the deposition process which reduced the number of reactive sites. Thus, the reduction in Ni^{2+} was inhibited to a certain extent, thereby reducing the deposition rate. However, as the glycine concentration further increased, the excess complex formed in solution increased the reduction difficulty and an insulating layer was formed as a result of more glycine molecules being adsorbed on the cathode surface, shown in Fig. 16c, blocking the continuity of electrodeposition and eventually decreasing the nickel deposition rate.

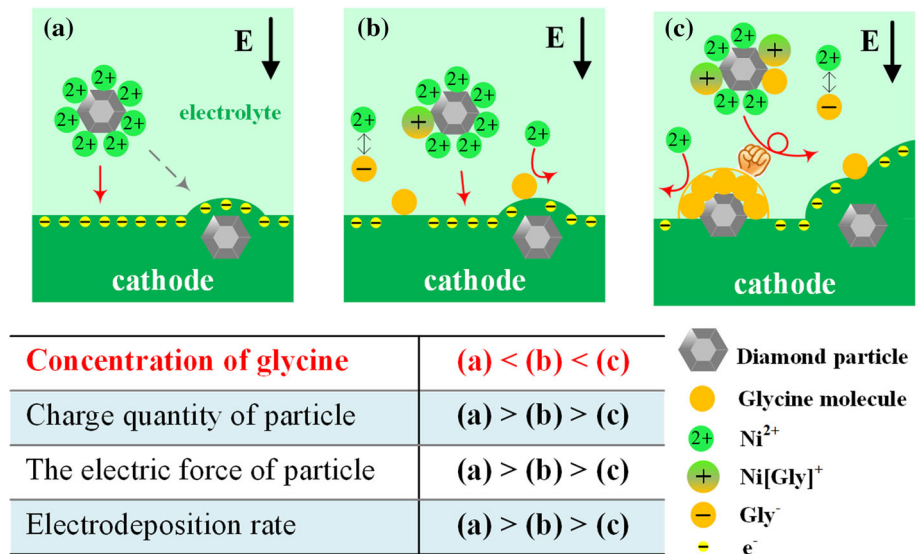In addition, because a complex ion only carried a single positive charge, the charge of the particles surrounded by complex ions tended to decrease with the increasing glycine, thus weakening the electric field force, which decreased the deposition rate of diamond particles, as listed in Fig. 16. Finally, the overall deposition rate showed a decrease, indicating that the inhibitory effects of glycine on the co-deposition rate were positively related to glycine concentration, which greatly reduced the deposition efficiency. This micromodel shown in Fig. 16 demonstrated that glycine had a regulatory effect on the co-electrodeposition rate.

Effects on microhardness

The high hardness of diamond particles has a strengthening effect on the nickel matrix through dispersion hardening, which improves the ability of a coating to resist plastic deformation [45, 46]. So the hardness of the composite coating is much higher than that of a pure nickel coating. The increased hardness of the composite coating may also be attributed to the effects of glycine on promoting grain refinement.

An electro-chemo-mechanical coupling micromodel about the composite coatings prepared by different glycine concentrations is shown in Fig. 17, which is based on the model of the electrochemical process shown in Fig. 16. When the bath was free of glycine (Fig. 17a), the grain size of the nickel matrix was larger with fewer grain boundaries, whereas the size of grains surrounding the diamond particles was

Figure 16 Micromodel of electrochemical process on cathode surface under different glycine concentrations.

Concentration of glycine	(a) < (b) < (c)
Charge quantity of particle	(a) > (b) > (c)
The electric force of particle	(a) > (b) > (c)
Electrodeposition rate	(a) > (b) > (c)

Diamond particle
Glycine molecule
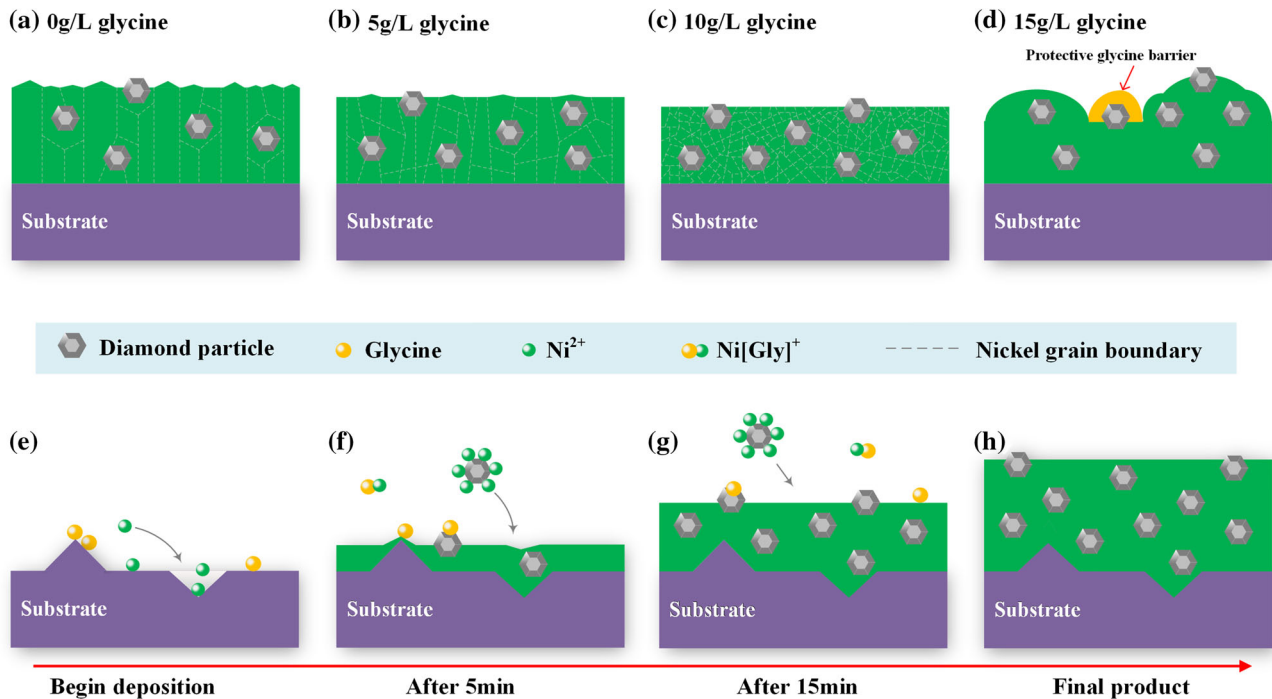Ni^{2+}
$Ni[Gly]^+$
Gly^-
e^-

Figure 17 Micromodel of composite coatings prepared at different glycine concentrations: (**a–d**); micromodel of the composite coating deposition process at 10 g L^{-1} glycine: (**e–h**).

smaller than that of other zones without diamond, possibly owing to the inhibiting effect on the growth of nickel nuclei caused by the inclusions or steric hindrance of inert diamond particles [23]. This effect promoted the growth of different crystal grains, leading to grain refinement. However, the average grain size of such nickel matrix was still relatively large (Fig. 8) and the microhardness of the composite coating was less than 400 HV (Fig. 11).

The addition of a moderate amount of glycine improved the quality of composite coating. As shown in Fig. 16b, a few free glycine molecules were randomly adsorbed onto the cathode surface, so that cathode active sites became more disperse. Thus, the growth of crystal nuclei was disturbed, which promoted new nucleation sites. Comparing the case without glycine as shown in Fig. 17a, the nickel grains became smaller and the number of grain boundary increased due to the addition of glycine, as shown in Fig. 17b, c.

This effect increased the hardness of the nickel matrix. The active sites were randomly occupied by glycine molecules, dispersing the diamond particles enveloped by the cations. The number of free glycine molecules increased with the glycine concentration

(Fig. 14). The glycine molecules adsorbed by the diamond particles partly embedded into the matrix prevented cations reduction, changing such exposed particle surface into inactive site. Thus, the suspended diamond particles enveloped by cations were oriented to the active sites (Fig. 16b), which in turn hindered the particles agglomeration and resulted in a more uniform distribution of diamond particles, enhancing the strengthening effect of diamond particles on the matrix nickel. When the glycine concentration was increased to 10 g L^{-1}, the microhardness of the composite coating reached its maximum, 580 HV.

However, the hardness showed no further increases as the glycine concentration was increased to 15 g L^{-1} for the following reasons. The excess complex reduced the charge of diamond particles and decreased the deposition rate of particles (Fig. 16c). Furthermore, a bulky diamond particle adsorbed too many glycine molecules, which could not be taken away by stirring in time, might form an insulating layer, which prevented the coating from depositing and gradually formed a pit in that local area. Then, an uneven coating surface was achieved and eventually resulted in the bulges and aggregation, as shown by

the results in Figs. 3e and 6e. Ultimately, the coating microhardness decreased as a result of the weak reinforcement by uneven diamond distribution in the nickel matrix. The composite coating achieved the highest microhardness when the glycine concentration was 10 g L^{-1}, as shown in Fig. 11.

In addition, the effect of glycine on coating hardness could also be explained by considering the system energy. An increase in glycine in the plating bath caused a negative shift in the cathodic polarization curve [34, 47], which increased the over-potential. That is, more energy was required from the power supply to activate the complex owing to its higher stability constant during the reduction reaction. It is well known that the smaller crystal nuclei have a higher surface free energy. Accordingly, the critical size of the nickel crystal nuclei was decreased to counteract the extra system energy. As the nucleation rate increased, the growth of crystal nuclei was retarded, resulting in grain refinement, as shown in Figs. 8 and 17a–c. Grain refinement could increase the coatings hardness based on the Hall–Patch effect [35], and glycine likely contributed to the improved hardness in this way.

Effects on roughness

Not only the grain refinement, but also the addition of glycine improves the roughness of the composite coating. Figure 17e–h describes the co-electrodeposition process at a glycine concentration of 10 g L^{-1}. At the beginning of the deposition, pits or grooves were created on the surface of the stainless steel substrate. The flow direction of the plating solution under

Figure 18 Flowchart for optimizing glycine concentration during the co-electrodeposition of Ni–diamond composite coatings.

stirring was perpendicular to the direction of the grooves, inducing that the glycine preferentially adsorbed to the higher protrusions of cathode surface and the nickel ions preferentially deposited in valleys (shown in Fig. 17e), which smoothed the cathode surface as shown in Fig. 17f. This procedure also enhanced the continuity of the interface between the film and substrate and consolidated the bonding strength. Meanwhile, the absorption of complex ions onto the diamond particles weakened the effects of the electric field on the particles, which promoted the glycine molecules to be randomly adsorbed on the cathode surface and disturbed the active sites, thus avoiding agglomeration of the dispersed particles. Hence, the distribution of the diamond particles in the composite coating became more uniform, shown in Fig. 17g. All above led to the formation of relatively flat coating surface, shown in Fig. 17h.

The trend above reversed when the glycine concentration was 15 g L^{-1}, as shown in Fig. 16c, because of excess glycine adsorbed on the angular surface of the diamond particles and the cathode surface, firming a local protective layer to hinder the further deposition, whereas the deposition continued in other areas, inducing an increase in surface roughness, as shown in Fig. 17d.

Effects on wear resistance

The diamond particles dispersing inside the composite coating reduced the direct contact between the nickel and the bearing ball, decreasing the wear of the composite coating during the friction process. During wearing, the diamond particles in the composite coating were continuously exposed and subjected to the bearing ball. Because the friction coefficient, μ, between the diamond and the bearing ball ($\mu = 0.16$) was far lower than that between the nickel and the bearing ball ($\mu = 0.44$) [25], the diamond particles reduced the shear force along the friction surface of the composite coating and the bearing ball [26]. A higher content and/or a more uniform distribution of diamond particles inside the nickel matrix gave the composite coating a lower friction coefficient and better wear resistance [27]. According to the analyses above, the content and uniformity of diamond particles showed a positive correlation with the glycine concentration until 10 g L^{-1}; hence, the Ni–diamond composite coating had its lowest friction coefficient (Fig. 12) and the highest diamond content (Fig. 5) at
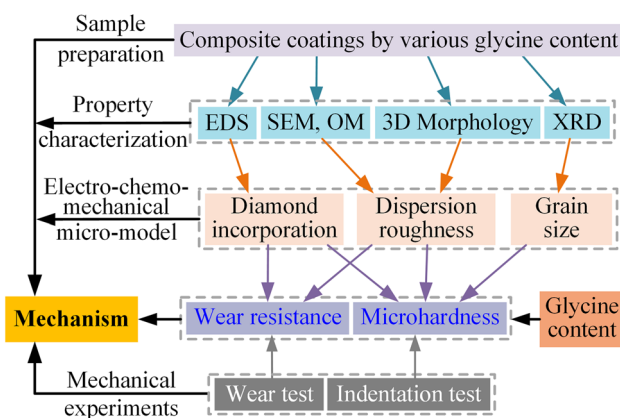
glycine concentration of 10 g L^{-1}. This result was also consistent with the wear resistance, which was positively related to the diamond content. When the glycine concentration reached 15 g L^{-1}, the inhibitive effect of excess glycine caused agglomeration of the diamond particles and the complex ions carrying a lower charge decreased the particle co-deposition rate, reducing the amount of particles in the composite coating and weakening the coating wear resistance. In one word, glycine plays an important role in the wear resistance of the composite coating (Fig. 13).

Conclusions

This paper presented an experimental work applying glycine as a new multifunctional additive to improve the mechanical properties of Ni–diamond composite coating deposited in a Watts-type bath. A flowchart for optimizing the glycine concentration during the co-electrodeposition of Ni–diamond composite coatings is proposed as shown in Fig. 18. The experimental results confirmed that the presence of glycine effectively improved the surface morphology, diamond particle content, and the roughness of the Ni–diamond composite coatings. Glycine complexation contributed to the grain refinement inside the microstructure of the coating and improved the dispersion of the diamond particles in the coatings, both of which made a positive contribution to the amount and uniformity of embedded diamond particles. The improvement of amount and uniformity then enhanced the microhardness, reduced the friction coefficient, and hence increased the wear resistance of the composite coatings, which was proved by wear testing under dry sliding condition. The wear resistance, diamond incorporation, and microhardness were all achieved their optimum conditions when the glycine concentration was 10 g L^{-1}.

Acknowledgements

References

[1] Huang W, Zhao Y, Wang X (2013) Preparing a high-particle-content Ni/diamond composite coating with strong abrasive ability. Surf Coat Technol 235:489–494

[2] Wang HT, Sheu HH, Hou KH, Ger MD (2014) Preparation and wear resistance of electrodeposited Ni–W/diamond composite coatings. Appl Surf Sci 308:372–379

[3] Ataie SA, Zakeri A (2016) Improving tribological properties of (Zn-Ni)/nano Al$_2$O$_3$composite coatings produced by ultrasonic assisted pulse plating. J Alloys Compd 674:315–322

[4] Zhou X, Shen Y (2014) A comparative study of pure nickel and the Ni-CeO$_2$ nanocrystalline coatings: microstructural evolution, oxidation behavior, and thermodynamic stability. J Mater Sci 49:3755–3774. https://doi.org/10.1007/s10853-014-8087-5

[5] Gyawali G, Kim HS, Tripathi K, Kim TH, Lee SW (2014) Fabrication and characterization of electrodeposited Ni-SiCh/BN composite coatings. J Mater Sci Technol 30:796–802

[6] Sajjadnejad M, Omidvar H, Javanbakht M, Mozafari A (2017) Textural and structural evolution of pulse electrodeposited Ni/diamond nanocomposite coatings. J Alloys Compd 704:809–817

[7] Ger MD (2004) Electrochemical deposition of nickel/SiC composites in the presence of surfactants. Mater Chem Phys 87:67–74

[8] Bełtowska-Lehman E, Góral A, Indyka P (2011) Electrodeposition and characterization of Ni/Al$_2$O$_3$ nanocomposite coatings. Arch Metall Mater 56:919–931

[9] Das MK, Li R, Qin J et al (2017) Effect of electrodeposition conditions on structure and mechanical properties of Ni-W/diamond composite coatings. Surf Coat Technol 309:337–343

[10] Hsue AWJ, Chang YF (2016) Toward synchronous hybrid micro-EDM grinding of micro-holes using helical taper tools formed by Ni-Co/diamond Co-deposition. J Mater Process Technol 234:368–382

[11] Zhang X, Qin J, Das MK et al (2016) Co-electrodeposition of hard Ni-W/diamond nanocomposite coatings. Sci Rep 6:1–11

[12] Jiang SW, Pang JN, Yang L, Lin H, Wang ZQ (2016) Electrodeposition of Ni-Al$_2$O$_3$ composite coatings with combined addition of SDS and HPB surfactants. Surf Coat Technol 286:197–205

[13] Chen L, Wang L, Zeng Z, Zhang J (2006) Effect of surfactant on the electrodeposition and wear resistance of Ni-Al_2O_3 composite coatings. Mater Sci Eng A 434:319–325

[14] Sabri M, Sarabi AA, Naseri Kondelo SM (2012) The effect of sodium dodecyl sulfate surfactant on the electrodeposition of Ni-alumina composite coatings. Mater Chem Phys 136:566–569

[15] Vaezi MR, Sadrnezhaad SK, Nikzad L (2008) Electrodeposition of Ni-SiC nano-composite coatings and evaluation of wear and corrosion resistance and electroplating characteristics. Coll Surf A Physicochem Eng Asp 315:176–182

[16] Zhou Y, Xie FQ, Wu XQ, Zhao WD, Chen X (2017) A novel plating apparatus for electrodeposition of Ni-SiC composite coatings using circulating-solution co-deposition technique. J Alloys Compd 699:366–377

[17] Choi Y, Kim D, Son K, Lee S, Chung W (2015) Effect of added dispersants on diamond particles in Ni-diamond composites fabricated with electrodeposition. Met Mater Int 21:977–984

[18] Wang J, Zhang FL, Zhang T, Liu WG, Li WX, Zhou YM (2018) Preparation of Ni-P-diamond coatings with dry friction characteristics and abrasive wear resistance. Int J Refract Met Hard Mater 70:32–38

[19] Aruna ST, Bindu CN, Ezhil Selvi V, William Grips VK, Rajam KS (2006) Synthesis and properties of electrodeposited Ni/ceria nanocomposite coatings. Surf Coat Technol 200:6871–6880

[20] Cioatera N, Samide A, Maxut A, Vannier R, Traisnel M (2011) Electrodeposition of ni-ceria nanocomposite coatings and their corrosion behavior. Rev Roum Chim 56:1003–1009

[21] Sen R, Sharma A, Bhattacharya S, Das S, Das K (2010) Synthesis and characterization of pulse co-electrodeposited nickel/ceria nanocomposites. J Nanosci Nanotechnol 10:4998–5003

[22] Fan LS, Constantin L, Li DW et al (2018) Ultraviolet laser photolysis of hydrocarbons for nondiamond carbon suppression in chemical vapor deposition of diamond films. Light Sci Appl 7:17177–17179

[23] Fan LS, Zhou YS, Wang MX, Gao Y, Liu L, Silvain JF, Lu YF (2014) Resonant vibrational excitation of ethylene molecules in laser-assisted diamond deposition. Laser Phys Lett 11:076002

[24] Lee EC, Choi JW (2001) A study on the mechanism of formation of electrocodeposited Ni-diamond coatings. Surf Coat Technol 148:234–240

[25] Lee WH, Tang SC, Chung KC (1999) Effects of direct current and pulse-plating on the co-deposition of nickel and nanometer diamond powder. Surf Coat Technol 120:607–611

[26] Zhou H, Du N, Zhu L, Shang J, Qian Z, Shen X (2015) Characteristics investigation of Ni-diamond composite electrodeposition. Electrochim Acta 151:157–167

[27] Ogihara H, Safuan M, Saji T (2012) Effect of electrodeposition conditions on hardness of Ni-B/diamond composite films. Surf Coat Technol 212:180–184

[28] Qin J, Zhang X, Xue Y, Kumar Das M, Thueploy A, Limpanar S, Liu R (2015) The high concentration and uniform distribution of diamond particles in Ni-diamond composite coatings by sediment co-deposition. Surf Interface Anal 47:331–339

[29] Wang Y, Yang C, He J, Wang W, Mitsuzake N, Chen Z (2016) Effects of choline chloride on electrodeposited Ni coating from a Watts-type bath. Appl Surf Sci 372:1–6

[30] Chung W, Lee S, Kim D, Son K, Choi Y (2016) Effect of propargyl alcohol on Ni-diamond composite electrodeposition for enhancing cutting performance. Korean J Met Mater 54:304–312

[31] Taranina OA, Evreinova NV, Shoshina IA, Naraev VN, Tikhonov KI (2010) Electrodeposition of nickel from sulfate solutions in the presence of aminoacetic acid. Russ J Appl Chem 83:58–61

[32] Lačnjevac U, Jović BM, Jović VD (2012) Electrodeposition of Ni, Sn and Ni–Sn Alloy coatings from Pyrophosphate-Glycine bath. J Electrochem Soc 159:D310–D318

[33] Sotskaya NV, Dolgikh OV (2008) Nickel electroplating from glycine containing baths with different pH. Prot Met 44:479–486

[34] Yang Y, Pan BS, Zhang YY (2017) Effect of glycine on properties of electroplated nickel coating. Mater Prot 50:69–72

[35] Trzaska M, Mazurek A (2016) Properties of nanocomposite Ni/diamond coatings produced by the electrocrystallization method. Compos Theory Pract 16:37–41

[36] Li X, Wei C, Yang Y (2005) Full field and microregion deformation measurement of thin films using electronic speckle pattern interferometry and array microindentation marker method. Opt Lasers Eng 43:869–884

[37] Mosavat SH, Bahrololoom ME, Shariat MH (2011) Electrodeposition of nanocrystalline Zn-Ni alloy from alkaline glycinate bath containing saccharin as additive. Appl Surf Sci 257:8311–8316

[38] Wang JS, Hsieh CC, Lai HH, Kuo CW, Wu TY, Wu W (2015) The relationships between residual stress relaxation and texture development in AZ31 Mg alloys via the vibratory stress relief technique. Mater Charact 99:248–253

[39] Van Huis MA, Van Veen A, Schut H et al (2002) Optical and structural properties of Li, Zn, Ag and Au nanoclusters embedded in MgO. Rev Adv Mater Sci 4:60–64

[40] Wang L, Gao Y, Liu H, Xue Q, Xu T (2005) Effects of bivalent Co ion on the co-deposition of nickel and nano-diamond particles. Surf Coat Technol 191:1–6

[41] Ibrahim MAM, Al Radadi RM (2015) Role of glycine as a complexing agent in nickel electrodeposition from acidic sulphate bath. Int J Electrochem Sci 10:4946–4971

[42] Bachmanna RT, Wiemkenac D, Tengkiatb AB, Wilichowskic M (2010) Feasibility study on the recovery of hexavalent chromium from a simulated electroplating effluent using Alamine 336 and refined palm oil. Sep Purif Technol 75:303–309

[43] Ergeneman O, Sivaraman KM, Pané S et al (2011) Morphology, structure and magnetic properties of cobalt-nickel films obtained from acidic electrolytes containing glycine. Electrochim Acta 56:1399–1408

[44] Guo J, Guo X, Wang S, Zhang Z, Dong J, Peng L, Ding W (2016) Effects of glycine and current density on the mechanism of electrodeposition, composition and properties of Ni-Mn films prepared in ionic liquid. Appl Surf Sci 365:31–37

[45] Hou KH, Ger MD, Wang LM, Ke ST (2002) The wear behaviour of electro-codeposited Ni-SiC composites. Wear 253:994–1003

[46] Mirzamohammadi S, Khorsand H, Aliofkhazraei M (2017) Effect of different organic solvents on electrodeposition and wear behavior of Ni-alumina nanocomposite coatings. Surf Coat Technol 313:202–213

[47] Ibrahim MAM, Al Radadi RM (2015) Noncrystalline cobalt coatings on copper substrates by electrodeposition from complexing acidic glycine baths. Mater Chem Phys 151:222–232